TURBULENT BOUNDARY LAYER OVER STRUCTURED POROUS SURFACE

Zhixiang Feng
Institute of Fluid Engineering
Zhejiang University
Hangzhou, 310027, China
fzx1998@zju.edu.cn

Qingqing Ye
Institute of Fluid Engineering
Zhejiang University
Hangzhou, 310027, China
qingqing_ye@zju.edu.cn

ABSTRACT

Porous media is a widely used passive flow control device, which shows potential in reducing skin friction and mitigating flow introduced noise. In the present study, structured porous media is applied to a flat plate to investigate its interaction with turbulent boundary layer. Cylindrical pores are uniformly distributed over the porous surface. The two-dimensional and three-dimensional flow field over the porous surface were respectively measured using planar and tomographic PIV at the momentum-based Reynolds numbers of 719. The flow field over smooth surface was also measured for comparison. The porous media induced momentum transport close to the wall, leading to the generation of alternative low- and high-speed regions. The streamwise velocity fluctuations decreases and the turbulence near the wall tends to be isotropic. While the coherence of streamwise velocity streaks reduced. Most streaks are located at the side of pores and migrate downstream.

INTRODUCTION

Porous media exists widely in nature, such as river beds, forest canopies and bird feathers. Inspired by the silent flight of owls, the porous media shows large potential in reducing flow induced noise, which is used as passive method for noise mitigation in aerospace and wind energy industry (Kroeger et al., 1971). In addition, the possibility of drag reduction is also found through the study of anisotropic porous media (Gómez-de-Segura and García-Mayoral, 2019).

In order to make better use of porous media to achieve noise and drag reduction and more optimized design, it is necessary to fully understand the influence of porous media on the boundary layer.

Suga et al. (2017) performed an experimental study on two-dimensional flow characteristics of turbulent boundary layer over metal foam in a rectangular pipe flow, and found that with the increase of permeability Reynolds number, the streak structures tend to fade. Ali et al. (2018) found that the use of porous media greatly changed the energy cascade distribution in the turbulent boundary layer, increased the pressure fluctuation on the wall and reduced the spanwise coherence length. Kim et al. (2018) studied the interaction of the flow across interface of porous media, using refractive-index matching and PIV technique to capture the flow overlying and within porous media. The results showed that the flow on both sides of the interface is negatively correlated. The crest region for the 5-layer case reduces stress close to the wall. However, the evolution of coherent structures over the porous surface is not fully understand yet, due to its three-dimensional intermittency nature.

Recent studies found that structured porous media has similar drag and noise reduction effect to the unstructured type (like ceramic and metal foam) (Carpio et al., 2020). The porosity and interior pattern of the structured is easier to control and design. In the present study, we used structured porous media with uniformly distributed circular pores on zero-pressure gradient flat plate. The porous media has arrays of circular through pores, with the diameter of 1 m. Time-resolved planar and tomographic PIV to capture the instantaneous flow features. The statistical and coherent structural analysis of the flow are performed.

EXPERIMENT SETUP

The experiments were carried out at the closed-loop wind tunnel in the Institute of Fluids Engineering, Zhejiang University. The wind tunnel has a cross-sectional area of 0.4×0.5 m^2. The contraction ratio of the tunnel is 6.2:1, resulting a maximum velocity of 35m/s.

A flat plate of 630 mm×400 mm×20 mm is installed over the symmetry plane of the test section, as shown in Figure 1. In order to inhibit flow separation, the leading-edge of the plate is designed using super-elliptical shape. The trailing edge of the plate ends with 12° inclination angle. The porous media of 100 mm×50 mm is installed at 378 mm downstream of the leading edge. Boundary layer trip is applied at 100 mm from the leading edge, achieving fully turbulent boundary condition before reaching the porous surface. The *x*, *y*, *z* axis corresponds to the streamwise, wall-normal and spanwise directions, originating from the start location of the porous media. The incoming velocity is 10 m/s. The Reynolds number based on momentum thickness of the boundary layer (Re_θ) at the porous location is 719.

(a)

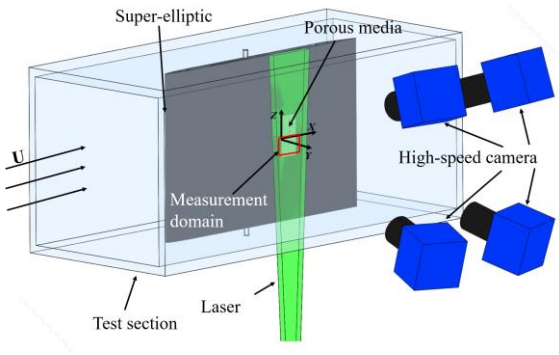

(b)

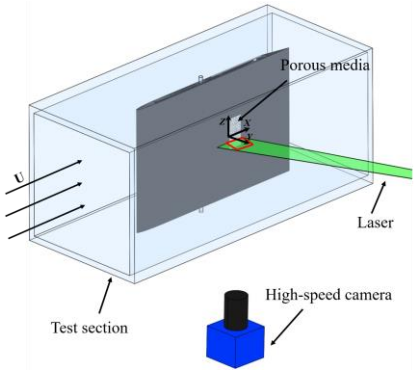

Figure 1. Schematic illustration of experimental setup. (a) Tomo-PIV and (b) Planar PIV.

Structured porous media are porous media with arrays of circular pores was used. One pore size of 2mm diameter was studied. The details of porous media arrangements are shown in Fig. 2 and Table 1. In addition, a solid surface insert was tested under the same flow conditions for comparison.

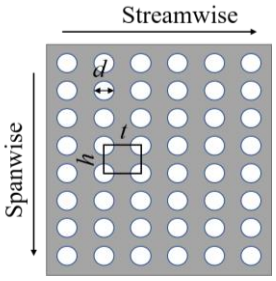

Figure 2. Porous media (diameter *d*, streamwise distance between adjacent pores *t* and streamwise distance between adjacent pores *h*)

Table 1. Porous media detail parameters

	h/mm	*t/mm*	*d/mm*
Smooth	——	——	——
Porous	4.6	4.2	2

The instantaneous velocity field is measured with time-resolved planar and tomographic PIV (Tomo-PIV). For the Planar-PIV (Fig. 1(b)), the measurement domain of 50×22 mm^2 (x×y) starts from 5 mm upstream of the porous media. Images were captured using a high-speed camera at the frequency of 2 kHz (Photron FASTCAM Mini AX100, 1024×1024 pixels). The illumination was provided by Beamtech Vlite-Hi-527-50 high speed laser (Nd:YLF, 527nm, 50 mJ/pulse at 1 kHz). The laser beam is converted into light sheet with a thickness of about 1 mm using an optical lens array. An ensemble size of dataset of 4000 was obtained.

For the tomo-PIV (Fig.1 (a)), the measurement domain of 40×4×40 mm^3 (x×y×z) locates in the range of x = [-8, 32] mm adjacent to the surface. Images are recorded using four high-speed cameras (two Photron FASTCAM SA4 and two Photron FASTCAM Mini AX100, 1024×1024 pixels) with cross arrangement. Each camera is equipped with objective of 105mm focal length and Scheimpflug adapters. The same laser device is used to provide the illumination and the laser beam is turned into light sheet with a thickness of 4 mm by using optical lens. The snapshots were acquired at 1.5 kHz with ensemble size of 500.

TIME-AVERAGED FLOW TOPOLOGY

The time-averaged flow topology is investigated to provide the first inspection on the interaction between porous surface and turbulent boundary layer. The cross-plane contour in x-y plane non-dimensional streamwise velocity and wall-normal velocity (u/u_∞ and v/u_∞ , respectively) were obtaining by averaging 4000 snapshots, as shown in Fig. 3. Contours of mean velocity difference ($\Delta u/u_\infty$) by subtracting the result over smooth surface is also presented in Fig. 3. The grey areas at the bottom of the image represent solid walls and the white areas represent pores. Streamlines are superimposed in the zoomed area to visualize the vortical structures. The influence of porous surface is actively present in the near wall region of y < 1mm. The mean velocity in the near wall region exhibits strong streamwise inhomogeneity over the porous surface. The pores induce strong upwash and downwash motion at the upstream and downstream half of each pore, respectively, shown by the wall-normal velocity in Fig. 3(b). The momentum transport of fluid leads to the formation of alternative high- and low-speed regions (Fig. 3(a)), which exist from the most upstream of pore centered at x = 1mm and sustains until the most downstream of the measurement domain. These phenomenon over the porous surface is consistent with previous researches (Kim et al., 2020). The intensity of downwash motion is remarkably higher than the upwash, leading to higher near wall streamwise velocity compared with smooth surface case (Fig. 3(c)). The results indicate the weakening of wall blocking effect (Breugem et al., 2006). The relaxation of the no-slip boundary condition leads to surface shear stress reduction. The magnitude of wall-normal velocity grows from v/u_∞ = 0.07 to 0.2 from upstream to downstream, revealing the enhancement of momentum transport across the porous surface.

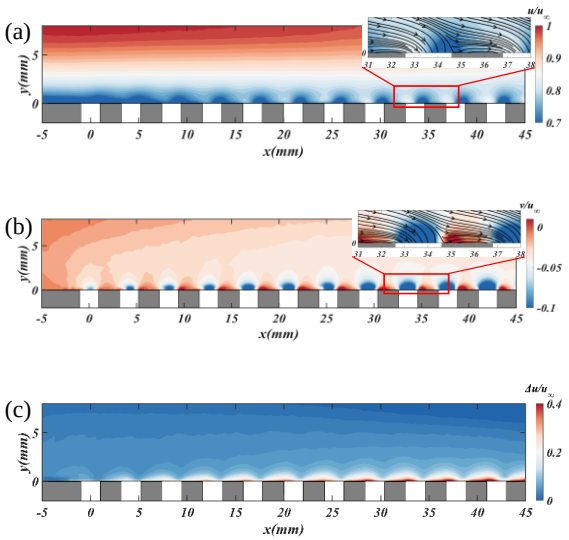

Figure 3. Time-averaged velocity field over the porous surface at x-y plane. (a) streamwise velocity (u/u_∞), (b) wall-normal velocity (v/u_∞), (c) mean streamwise velocity difference ($\Delta u/u_\infty$), (d) mean wall-normal velocity change. The flow topology is shown by the zoomed red rectangle area superimposed with streamlines. The grey areas represent solid walls and the white areas represent pores.

To further understand the influence of the porous media on the turbulent boundary layer, the three-dimensional time-averaged flow field closed to porous surface is illustrated in Fig. 4. For each pore, a pair of counter-rotating streamwise vortices locate at the side flank (Fig. 4(a)), leading to the modification of mean boundary layer in not only streamwise but also spanwise directions. The intensity of the counter-rotating vortice increases when developing downstream. Besides the downwash motion over the pores, the vortex pair induce strong upwelling motion between spanwise neighboring pores, which cause the low-momentum fluid to move away from the wall and generate low-speed regions, as shown by the *y*-*z* plane in Fig. 4(b). The low-speed area extends in the streamwise direction over the entire measurement domain due to the successive upwash motion, bounding the high-speed regions over the pores, as shown in Fig. 4(c). This phenomenon has also been observed in the mean flow field over rough surfaces, which is caused by large-scale secondary flows (Barros et al., 2014). Mejia-Alvarez and Christensen (2013) refers to the low-speed elongated area after time average as the low-momentum pathway (LMP), differing from the low-momentum region (LMR) detected in instantaneous velocity field of wall turbulence. The LMR is associated to the growth of Kelvin-Helmholtz (K-H) instability, leading to the formation of large scale-hairpin structures. The latter will be discussed in the remaining study.

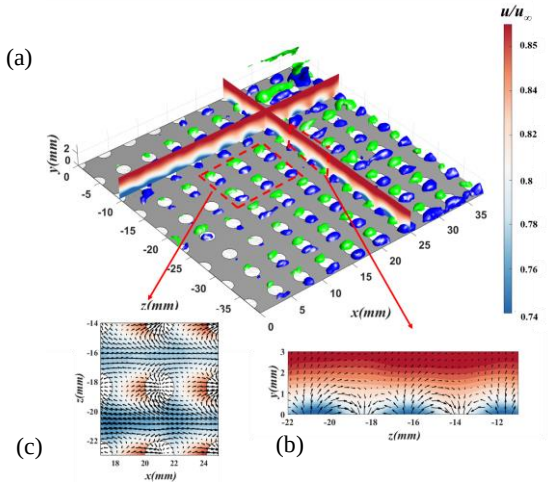

Figure 4. Three-dimensional time-averaged flow field near the porous surface. Iso-surfaces represent the time-averaged streamwise vorticity ($\omega_x = \pm 300\ 1/s$). Cross planes contours of the time-averaged streamwise velocity are shown at *y*-*z* plane (b) and *x*-*z* plane at y = 0.15 mm (c).

TURBULENT FLUCTUATIONS

In order to quantitatively analyze the effect of momentum transport induced by the porous surface to the turbulent fluctuations, R.M.S. of the streamwise and wall-normal velocity fluctuations ($<u'>/u_\infty$ and $<v'>/u_\infty$) are extracted at selected location, corresponding to pore, pore interval, and smooth surface, as shown in Fig. 5.

Compared with the smooth surface case, the streamwise velocity fluctuations ($<u'>/u_\infty$) decreases over the entire boundary layer for the porous surface case (Fig. 5(a)). The maximum reduction establishes close to the wall due to the relaxation of no-slip boundary condition over porous surface. This phenomenon has been observed in many studies of turbulent structures over metal foam (Manes et al., 2011; Suga et al., 2010) over the permeable walls comprised of regularly packed spheres (Kim, 2019). Manes et al. (2011) speculated that the reduction of $<u'>/u_\infty$ is related to the suppression of streaks near the wall over porous surface. This is confirmed by the absence of streaks over porous surface in the instantaneous 3D flow filed, which will be analyzed in detail below.

The decrease of the amplitude of $<v'>/u_\infty$ over porous surface is observed in the range of $0.15 < y/\delta_{99} < 0.5$ (Fig. 5(b)). This phenomenon was reported by Bhat et al. (2021) who performed a micro-cavity array to control the near-wall turbulence. It is worth mentioning that v_{rms}/u_∞ directly above the pores is bigger than that over smooth surface near the wall ($0 < y/\delta_{99} < 0.15$) due to the momentum exchange in the vertical direction (Kim et al., 2018). This result is in agreement with the near-wall intensity increase for the rms wall-normal velocity over porous media (metal foam) (Manes et al., 2011; Suga et al., 2010).

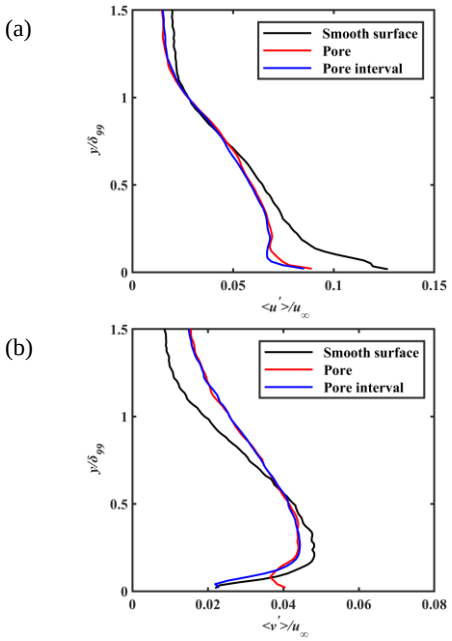

Fig 5 Profiles of streamwise and wall-normal velocity fluctuations. The black line represents smooth surface; the red and blue lines represent the pore location at x = 21mm and downstream interval at x = 23.1mm, respectively.

QUADRANT ANALYSIS

The sweep and ejection events induced by the porous surface by the quadrant analysis. The distribution of the joint probability density of the velocity fluctuations (u', v') at y = 0.45 mm ($y^+ \approx 12$) is depicted Fig 6. The density distribution above and the pore at x = 42mm and the interval directly downstream are shown in Fig 6(b) and (c) respectively. The solid red ellipse is the distribution profile with a confidence level of 95%. The shape profile of the joint probability density distribution yields ellipse for both the porous and the smooth surface. Both Q2 (ejection) and Q4 (sweep) events dominate the production of turbulence, while Q1 and Q3 events are secondary. However, compared with slender elliptical shape of the probability density distribution on the smooth surface (Fig 6a), the shape on the porous surface becomes 'round-shaped' and tilted (Fig 6b). This change in the shape indicates that the porous surface leads to the decrease of streamwise

velocity fluctuations (u') and slight increase of wall-normal velocity fluctuations (v') due to the momentum transport. The phenomenon is consistent with results of $<u'>/u_\infty$(Fig 5(a)) and $<v'>/u_\infty$ (Fig 5(b)) near the wall. Manes et al. (2011) observed similar change of velocity fluctuations in the near wall of the porous surface. Moreover, the distribution of the probability density over the pore interval (Fig. 6(c)) is still slender elliptical shape. However, the amplitude of$<u'>/u_\infty$decreases, while the amplitude of $<v'>/u_\infty$has little change. Similar results can be found in profiles of $<u'>/u_\infty$ (Fig. 5(a)) and $<v'>/u_\infty$ (Fig. 5(b)) over the pore interval. The block effect of the pore interval of porous surface prevents the flow from penetrating into the wall and causes the near-wall v'/u_∞ to return to the same level as in the smooth surface condition. The change in shape into round over porous surface indicates that the porous treatment turns the anisotropic turbulence over smooth surface into the less anisotropic turbulence, which is similar to observation of Suga et al. (2011).

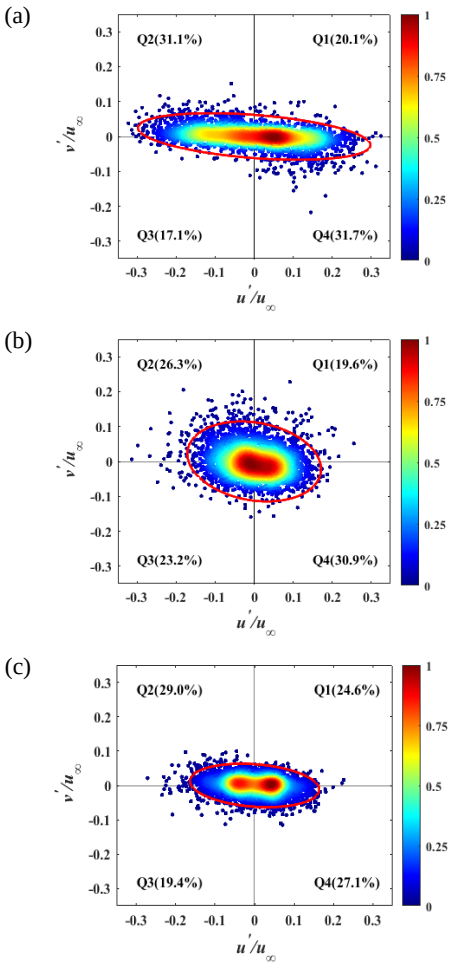

Figure 6. Quadrant analysis at y = 0.45 mm ($y^+ \approx 12$), coloured by the joint density distribution. The red circle highlights the profile of overall density distribution. (a) smooth surface, porous surface (b) at x = 42 mm and (c) at x = 44.1 mm.

COHERENT STRUCTURES

The evolution of three-dimensional coherent structures is represented by the streasmwise velocity streaks, which are identified as negative and positive streamwise velocity fluctuations. Iso-surfaces of streamwise velocity fluctuations (u'/u_∞ = ±0.1) are shown in Fig. 7, where green and blue represent the high- and low-speed streaks, respectively. Above the smooth surface, the streamwise elongated streaky structures with alternating sign along spanwise direction are clearly observed, which is consistent with the typical structures in a zero-pressure-gradient boundary layer (Kline et al., 1967). Although there are streamwise elongated streaks over the porous surface, the number of streaks is reduced and the quasi-periodic variation of streaks along the spanwise direction is suppressed. This phenomenon can be observed on both low-permeability surface (Suga et al., 2017) and high-permeability surface (Kuwata & Suga, 2019). The enhanced wall-normal upwash and downwash motion over porous surface (Fig. 3(b)) leadind to the growth of the K-H instability. The latter interrupts the streak formation. Notably, there are no apparent lager-scale spanwise rolls over the porous surface, which are generated by the K-H instability. The reason for this is that low wall-normal permeability and streamwise impermeability prevent development of the streamwise perturbation by the K-H instability. Another explanation is the instantaneous streamwise fluctuations can not well reflect the spanwise structure over porous surface and instead the pressure fluctuations might be a better option to show spanwise structures (Kuwata & Suga, 2016).

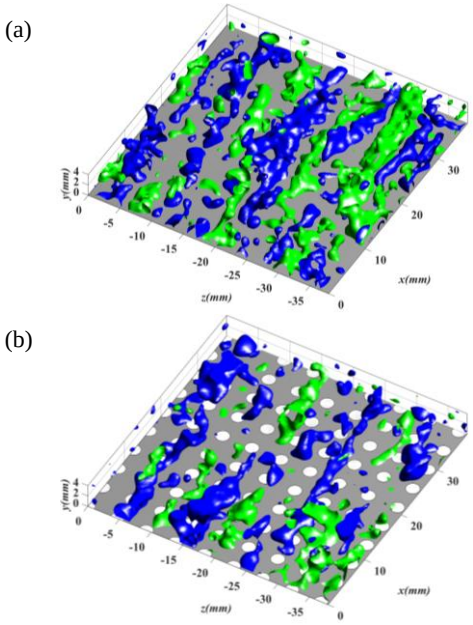

Figure 7. Iso-surfaces of instantaneous streamwise velocity fluctuations (u'/u_∞ = ±0.1). (a) smooth surface and (b) porous surface. The green and blue represent high- and low-speed streaks.

In order to quantitatively discuss the change of streak structure observed above, the two-point correlation analysis of streamwise velocity fluctuations at y = 0.31 mm ($y^+ \approx 10$) is performed, as shown in Fig. 8. The profile of correlation coefficient is obtained by global averaging. For two surfaces, the spanwise correlation coefficient drops to a negative peak at $\Delta z^+ \approx 93$, which is the mean spanwise length between neighboring high- and low-speed streaks. The streaks spacing of 93 wall units is close to that of 100 wall units over a smooth

surface by Kim et al. (1987). It can be inferred that the porous surface has little effect on the statistical spatial size of streaks, which is inconsistent with results for flow over an anisotropic porous surface with drag reduction (Li et al., 2020; Rosti et al., 2018). However, for the spanwise correlation coefficient, the magnitude of the negative peak over porous surface is smaller than that over smooth surface. The phenomenon shows that streamwise streaks over porous surface are less-organized (Suga et al., 2017), that is, the coherence between the low-speed streak and its adjacent high-speed streak is weakened.

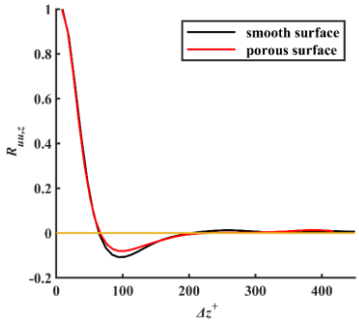

Figure 8. Two-point correlation of streamwise velocity fluctuations along spanwise.

LOW ORDER RECONSTRUCTION OF VELOCITY FIELD

The proper orthogonal decomposition (POD) is an effective method to extract the large-scale structure of the flow from turbulent flow. The background noise from PIV measurements and the influence of small-scale structures can be better removed, so that the spatial distribution characteristics of the large-scale coherent structures in the flow can be observed more clearly. In order to further study the effect of porous media on the turbulent boundary layer, low-order modes with cumulative energy reaching 90% ware selected to reconstruct the large-scale flow for three-dimensional velocity fields, as shown in Fig. 9. Since the high-speed streaks are not the main structure over the porous surface, only the low-speed strip structure is shown in the Fig. 9 for the sake of clarity. Fig 9(b) shows vortical structures in the red box area in Fig. 9(a).

Although the coherency of velocity streaks is reduced by the porous surface, there are still large-scale low-speed streaks in streamwise direction. Vortical structures surrounding low-speed streaks are also clearly captured, as shown in Fig. 9(b). By comparing the position of pores and low-speed streaks, it can be found that streaks appear on one side of pores. This phenomenon exists for both large-scale and relatively small-scale low-speed streaks. The instantaneous low-speed regions distribution is consistent with the time-averaged low-speed regions distribution (Fig. 4). This finding supports the previous hypothesis that the low-momentum pathways (LMPs) could be preferential pathways for instantaneous large-scale motions (LMRs) (Mejia-Alvarez & Christensen, 2013). The streamwise elongated streaks become less curvy over porous surface compared with that over smooth surface, which is consistent with flow over an anisotropic porous wall with drag reduction (Li et al., 2020). The arrangement of the pores in this paper induces large-scale secondary flow, which is responsible for the less curved streaks in the streamwise direction. However, the large-scale secondary flow that exists in the mean field is not observed in the instantaneous flow field. Vanderwel et al.'s (2019) explanation for this is that the large-scale secondary flow structures in the mean field are the time-averaged result of small-scale counter-rotating vortex pairs with stronger vorticity in the instantaneous flow fields. Moreover, very large-scale low-speed regions with surrounding vortical structures are convected downstream along the side of pores. That is to say, the vortical structures are concentrated on one side of pores, which is different from position of vortical structures over smooth surface. Similar distributions of vortical structures are observed in flows over smooth surfaces with spanwise heterogeneities (Ni et al., 2018).

(a)

(b)

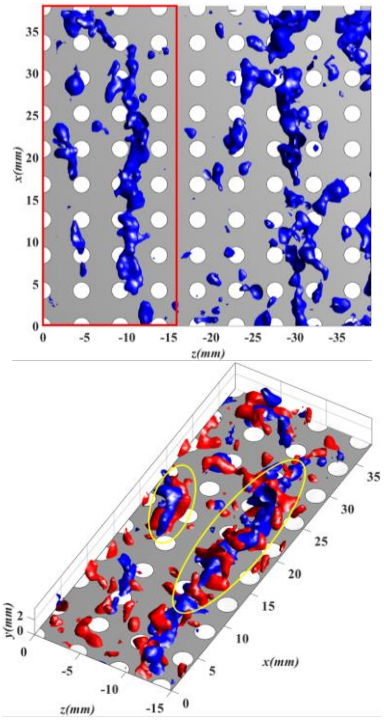

Figure 9. Iso-surfaces of instantaneous streamwise velocity fluctuations ($\boldsymbol{u}'/\boldsymbol{u}_\infty$= -0.1) and vortical structures (λ_{c_i} = 900) over porous surface reconstructed by low-order modes. (a) Top view of low-speed streaks and (b) vortical structures. The red iso-surface λ_{c_i} of represents vortical structures; the blue is low-speed streaks. The yellow circle highlights the coherent structures.

CONCLUSION

Structured porous media have great potential in noise and drag reduction. In order to study the mechanism of these functions, the instantaneous flow structures of turbulent boundary layer over porous surface are obtained by time-resolved planar and tomographic PIV. The porous surface with cylindrical pores is applied. The results show that the porous surface has resulted in the increase of the streamwise velocity near the wall and reduction of the turbulent intensities in the range of $0.15 < y/\delta_{99} < 0.5$. The joint probability density analysis of velocity fluctuation shows that the turbulence in the near-wall region of the porous surface tend to be isotropic. For the coherent structures, the streamwise velocity streaks over the porous surface are significantly suppressed and the distribution of the pores introduces the secondary flow, which causes the streaks less curevd and migrating downstream along the side of pores.

REFERENCES

Adrian, R. J., Meinhart, C. D., & Tomkins, C. D. 2000, "Vortex organization in the outer region of the turbulent boundary layer", *Journal of Fluid Mechanics*, Vol. 422, pp. 1-54.

Breugem, W. P., Boersma, B. J., & Uittenbogaard, R. E. 2006, "The influence of wall permeability on turbulent channel flow", *Journal of Fluid Mechanics*, Vol. 562, pp. 35-72.

Barros J M, Christensen K T., 2014, "Observations of turbulent secondary flows in a rough-wall boundary layer", *Journal of Fluid Mechanics*, Vol. 748, R1.

Bhat S S, Silvestri A, Cazzolato B S, et al., 2021, "Mechanism of control of the near-wall turbulence using a micro-cavity array", *Physics of Fluids*, Vol. 33(7), 075114.

Carpio, A. R., Avallone, F., Ragni, D., Snellen, M., & van der Zwaag, S. 2020, "Quantitative criteria to design optimal permeable trailing edges for noise abatement", *Journal of Sound and Vibration*, Vol. 485, 115596.

Gómez-de-Segura, G., Sharma, A., & García-Mayoral, R. 2018, "Turbulent drag reduction using anisotropic permeable substrates", *Flow, Turbulence and Combustion*, Vol. 100(4), pp. 995-1014.

Kline S J, Reynolds W C, Schraub F A, et al., 1967, "The structure of turbulent boundary layers". *Journal of Fluid Mechanics*, Vol. 30(4), pp. 741-773.

Kim J, Moin P, Moser R., 1987, "Turbulence statistics in fully developed channel flow at low Reynolds number", *Journal of Fluid Mechanics*, Vol. 177, pp. 133-166.

Kroeger, R. A., Grushka, H. D., & Helvey, T. C., 1972, "Low speed aerodynamics for ultra-quiet flight", *Tennessee Univ Space Inst Tullahoma*.

Kim, T., Blois, G., Best, J. L., & Christensen, K. T., 2018, "Experimental study of turbulent flow over and within cubically packed walls of spheres: Effects of topography, permeability and wall thickness", *International Journal of Heat and Fluid Flow*, Vol. 73, pp. 16-29.

Kim T.,2019, *Experimental investigation on turbulent flow overlying permeable walls*, Ph.D, University of Illinois at Urbana-Champaign.

Kuwata Y, Suga K., 2016, "Lattice Boltzmann direct numerical simulation of interface turbulence over porous and rough walls", *International Journal of Heat and Fluid Flow*, Vol. 61, pp. 145-157.

Kuwata Y, Suga K., 2019, "Extensive investigation of the influence of wall permeability on turbulence", *International Journal of Heat and Fluid Flow*, Vol. 80, 108465.

Li Q, Pan M, Zhou Q, et al., 2020, "Turbulent drag modification in open channel flow over an anisotropic porous wall", *Physics of Fluids*, Vol. 32(1), 015117.

Manes C, Poggi D, Ridolfi L., 2011, "Turbulent boundary layers over permeable walls: scaling and near-wall structure", *Journal of Fluid Mechanics*, Vol. 687, pp. 141-170.

Mejia-Alvarez R, Christensen K T., 2013, "Wall-parallel stereo particle-image velocimetry measurements in the roughness sublayer of turbulent flow overlying highly irregular roughness", *Physics of Fluids*, Vol. 25(11), 115109.

Ni W, Lu L, Fang J, et al., 2018, "Large-scale streamwise vortices in turbulent channel flow induced by active wall actuations", *Flow, Turbulence and Combustion*, Vol. 100(3), pp. 651-673.

Rosti M E, Brandt L, Pinelli A., 2018, "Turbulent channel flow over an anisotropic porous wall–drag increase and reduction", *Journal of Fluid Mechanics*, Vol. 842, pp. 381-394.

Suga K, Matsumura Y, Ashitaka Y, et al., 2010, "Effects of wall permeability on turbulence", *International Journal of Heat and Fluid Flow*, Vol. 31(6), pp. 974-984.

Suga, K., Mori, M., & Kaneda, M., 2011, "Vortex structure of turbulence over permeable walls", *International Journal of Heat and Fluid Flow*, Vol. 32(3), pp. 586-595.

Suga, K., Nakagawa, Y., & Kaneda, M., 2017, "Spanwise turbulence structure over permeable walls", *Journal of Fluid Mechanics*, Vol. 822, pp. 186-201.

Showkat Ali, S. A., Azarpeyvand, M., Szőke, M., & Ilário da Silva, C. R., 2018, "Boundary layer flow interaction with a permeable wall", *Physics of Fluids*, Vol. 30(8), 085111.

Vanderwel C, Stroh A, Kriegseis J, et al., 2019, "The instantaneous structure of secondary flows in turbulent boundary layers", *Journal of Fluid Mechanics*, Vol. 862, pp. 845-870.